PL-TR-95-2045

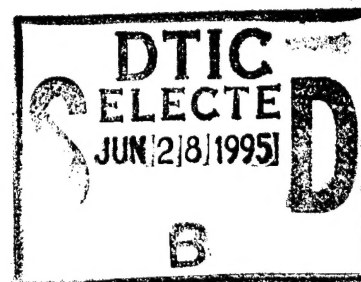# DETAILED COMPONENT DESIGN FOR A COMPACT ENVIRONMENTAL ANOMALY SENSOR (CEASE): MECHANICAL DESIGN AND CALIBRATION

Bronislaw K. Dichter
John O. McGarity
Alan C. Huber
John A. Pantazis
Valentin Jordanov

David Sperry
Hugh Anderson
Douglas Potter
Lorraine Johnson

AMPTEK, INC.
6 De Angelo Drive
Bedford, MA 01730

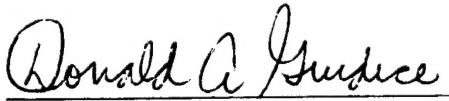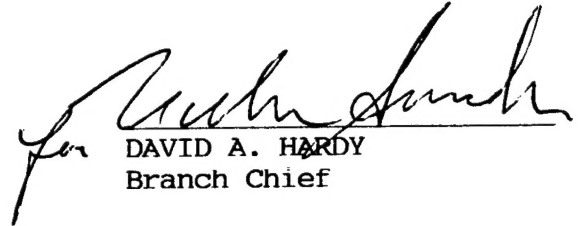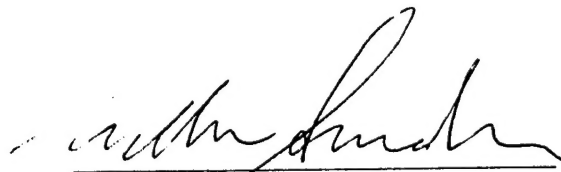17 April 1995

Scientific Report No. 4

PHILLIPS LABORATORY
Directorate of Geophysics
AIR FORCE MATERIEL COMMAND
HANSCOM AFB, MA 10731-3010

19950626 078

This technical report has been reviewed and is approved for publication.

DONALD A. GUIDICE
Contract Manager

for DAVID A. HARDY
Branch Chief

WILLIAM SWIDER
Deputy Division Director

REPORT DOCUMENTATION PAGE

Public reporting burden for this collection of information is estimated to average 1 hour per response, including the time for reviewing instructions, searching existing data sources, gathering and maintaining the data needed, and completing and reviewing the collection of information. Send comments regarding this burden estimate or any other aspect of this collection of information, including suggestions for reducing this burden, to Washington Headquarters Services, Directorate for Information Operations and Reports, 1215 Jefferson Davis Highway, Suite 1204, Arlington, VA 22202-4302, and to the Office of Management and Budget, Paperwork Reduction Project (0704-0188), Washington, DC 20503.

1. AGENCY USE ONLY (Leave blank)	2. REPORT DATE 17 April 1995	3. REPORT TYPE AND DATES COVERED Scientific No. 4

4. TITLE AND SUBTITLE

Detailed Component Design for a Compact Environmental Anomaly Sensor (CEASE): Mechanical Design and Calibration

5. FUNDING NUMBERS

PE 63410F
PR 2823   TA 01   WU AC

Contract F19628-90-C-0159

6. AUTHOR(S)

Bronislaw K. Dichter   John A. Pantazis   * Hugh Anderson
John O. McGarity   Valentin T. Jordanov   * Douglas Potter
Alan C. Huber   David J. Sperry   * Lorraine Johnson

7. PERFORMING ORGANIZATION NAME(S) AND ADDRESS(ES)

AMPTEK, Inc.
6 De Angelo Drive
Bedford, MA 01730

8. PERFORMING ORGANIZATION REPORT NUMBER

9. SPONSORING / MONITORING AGENCY NAME(S) AND ADDRESS(ES)

Phillips Laboratory
29 Randolph Road
Hanscom AFB, MA 01731-3010

Contract Manager: Donald Guidice/GPSG

10. SPONSORING/MONITORING AGENCY REPORT NUMBER

PL-TR-95-2045

11. SUPPLEMENTARY NOTES

* SAIC NW, 13400B Northrup Way, Suite 36, Bellevue, WA 98005

12. DISTRIBUTION / AVAILABILITY STATEMENT

Approved for public release. Distribution unlimited.

12b. DISTRIBUTION CODE

13. ABSTRACT (Maximum 200 words)

The outer space environment experienced by a modern, electronically sophisticated spacecraft can be very hostile due to interactions between its complex, sensitive electronics systems and the naturally occurring energetic particle population indigenous to the solar system. The Compact Environmental Anomaly Sensor (CEASE) is being developed as a small, low-power device to monitor space "weather" and provide autonomous warnings of conditions that may cause operational anomalies in a host spacecraft. CEASE uses a two-element solid-state telescope and two radiation dosimeters to sample critical energetic particle fluxes and uses a sophisticated real-time processing program that can forecast hazardous environmental conditions before they effect the spacecraft. The spacecraft, in turn, can re-prioritize its operations, inhibit any anomaly sensitive operations such as attitude adjustments, or take any other prudent action suggested by the potential of erratic conditions. The CEASE instrument is forecast to be packaged as a 4-inch cube weighing less than 3 pounds and dissipating less than 3 watts.

DTIC QUALITY INSPECTED 3

14. SUBJECT TERMS

Compact Environmental Anomaly Sensor, CEASE, Surface Charging, Deep Dielectric Charging, Single Event Upsets, Radiation Dose Effects.

15. NUMBER OF PAGES

22

16. PRICE CODE

17. SECURITY CLASSIFICATION OF REPORT	18. SECURITY CLASSIFICATION OF THIS PAGE	19. SECURITY CLASSIFICATION OF ABSTRACT	20. LIMITATION OF ABSTRACT
Unclassified	Unclassified	Unclassified	SAR

Table of Contents

List of Tables

List of Figures

iii

1. INTRODUCTION

The instrument CEASE (Compact Environmental Anomaly Sensor) is designed to detect conditions that may cause anomalies, that is, occurrences that may adversely affect spacecraft operation. It will do so before these conditions become so severe that anomalies actually occur and will provide warnings or flags on which spacecraft may act to protect themselves. These anomalies are:

Body charging occurs when the spacecraft chassis accumulates electrical charge and the whole space frame must rise to a significant potential (with respect to the surrounding plasma) in order to null the net current to it. This charging occurs even when the whole spacecraft surface is conducting and electrically connected. Body charging is caused by spacecraft emitting charge, such as in a particle beam, or when they are bombarded by kilovolt electrons such as the auroral electron flux or the hot plasma in GEO. The charging can become significant in the absence of neutralizing currents such as cooler plasma or photoelectrons ejected by sunlight.

Differential charging occurs under the same conditions as body charging if the spacecraft exterior has sections of electrically isolated conductors. As different portions of the surface experience different currents, these separate sections may reach different equilibrium potentials.

Surface dielectric charging occurs when somewhat penetrating particles bombard exposed dielectrics and stop in them. If the rate of charge buildup exceeds leakage through the dielectric, the resulting charge density may produce a very strong electric field that eventually breaks down the dielectric. Leakage depends upon the dielectric material; hence, charging may be cumulative over minutes up to many hours. Leakage increases as conductivity is enhanced by the effect of the bombarding particles. Consequently, protons are not very effective in causing dielectric charging because they readily increase dielectric conductivity. In addition, sunlight may help discharge very shallow deposits of charge. The result of these factors is that surface charging occurs when the electron flux exceeds a threshold value and sums to a fluence that exceeds a threshold.

Deep dielectric charging is produced in the same way as surface dielectric charging except that the causative electrons have enough energy to penetrate some distance into the dielectric. In some cases they may reach dielectrics that are behind conductors. An example of a buried dielectric is the insulator within a coaxial cable. Obviously, the energy boundary that divides surface and deep charging particles is somewhat arbitrary. Sunlight does not mitigate deep dielectric charging.

Total radiation dose is measured by the energy deposited in materials by charged particles passing through them. Dosage results from the totality of ionizing radiation that reaches the site of interest and is thus strongly affected by surrounding shielding. Sufficiently high levels can damage most materials, including dielectrics and optical materials. In most cases

semiconductors are the most sensitive elements on a spacecraft. Some devices experience degradation at tens of kilorads, while radiation hard devices can tolerate 10 to 100 times more. Dosage is mostly cumulative, as semiconductors self heal only a little.

Single event upsets (SEUs) result when an ionizing particle leaves enough charge (equivalently energy) in the sensitive volume of a semiconductor device to flip the logical state of the device. Generally, there is no permanent damage. The sensitive volumes are of micron size, and the required energy is 1 to 100 MeV depending upon the device. Neither electrons or protons have high enough LET (Linear Energy Transfer) to leave so much energy in a small volume. Only more highly charged particles such as alphas (in some cases) and $Z > 2$ particles can do this. However, protons that have nuclear collisions (called stars from their appearance in photographic film) in the sensitive volume can break up a nucleus and the resulting fragments leave enough energy to cause SEUs. Protons are so much more numerous than heavier particles that these nuclear collisions are the principal cause of SEUs.

The strategy that has evolved for a successful CEASE instrument consists of making a limited number of high-energy particle measurements using a pair of dosimeters and a solid-state telescope. We believe that if the right radiation parameters are sampled, then these data may be interpreted to identify and forecast environmental conditions that may affect the operation or longevity of a spacecraft. In the previous Scientific Report (PL-TR-94-2132), we presented the results of our work to optimize the instrument measurements to provide the required spacecraft hazard warning in a variety of space environments. This report contains the description of the instrument design developed as a result of the previous three year's work and some preliminary calibration and testing work that has been carried out using prototype CEASE sensors.

2

2. CEASE MECHANICAL DESIGN

The mechanical design of the CEASE instrument has been finalized. CEASE will be contained in an aluminum enclosure 4 in x 4 in (10 cm x 10 cm) in cross section and 3.2 in (8.1 cm) in height. The mass of the instrument will be less than 2.2 lb (0.98 kg). There will be six 3.5 in x 3.5 in printed circuit boards (PCB) in the instrument. The instrument sensor complement will consist of two dosimeters, one SEU detector and a two detector solid state telescope.

The topmost PCB (DOS), located about 0.25 in below the top cover has the two dosimeter detectors and the front end electronics for these sensors. The top cover has a 0.25 in thick Al degrader (35 MeV proton threshold) over one dosimeter detector and 0.08 in (20 MeV proton threshold) over the other one. The bottom end of the telescope assembly is mounted to the next PCB (TEL) which also contains the telescope front end electronics. The top end of the telescope is attached to the top cover. The SEU detector, and its front end electronics, is also located on the TEL PCB. The third board down (DSP) contains the analog-to-digital converter and the digital circuits needed to process the detector signals. The next board (µP) contains the microprocessor controlling the instrument, the system memory and associated circuits. The fifth PCB (I/O) will contain the spacecraft interface circuitry for the instrument. Although the µP and I/O boards could be combined into a single PCB, we have chosen to keep them separate to allow for easier I/O modifications when CEASE has to be adapted to a variety of different spacecraft. The bottom PCB (PS) will contain the DC/DC converters that provide the voltages required by the electronics and the high voltages required to bias the detectors.

The CEASE dosimeter detectors are 500 µm thick, 81 mm^2 area Si p-i-n detectors. Since the sensitive volume of the detectors is known, the measured energy deposition by incident particles can be converted to a dose in rads (Si). In addition, the different patterns of energy deposition in the detectors by incident electrons and protons can be used to distinguish the radiation doses due to electrons from those due to protons. The summed electron and proton counts can also be used to estimate the integral fluxes of these particles above energy thresholds set by the degraders.

The CEASE telescope is used to collect data on fluxes of energetic electrons (0.05 to 1 MeV) and low energy protons (2 to 15 MeV). These data are used to determine the spacecraft charging hazards and the radiation dose received by unshielded components such as solar panels (surface dose). Measured fluxes of electrons and protons in various energy ranges are converted to hazard warnings by the algorithms in the on-board microprocessor.

The telescope consists of two co-axially mounted Si solid state detectors. The front detector (DFT) is 150 µm thick and has a 25 mm^2 sensitive area, while the back detector (DBT) is 700 µm thick and has a 50 mm^2 sensitive area. The signals from each detector are amplified separately, but a coincidence circuit with a resolution time of 500 ns identifies true coincidence events for additional processing. A schematic cross-sectional diagram of the telescope is shown in Figure 1.
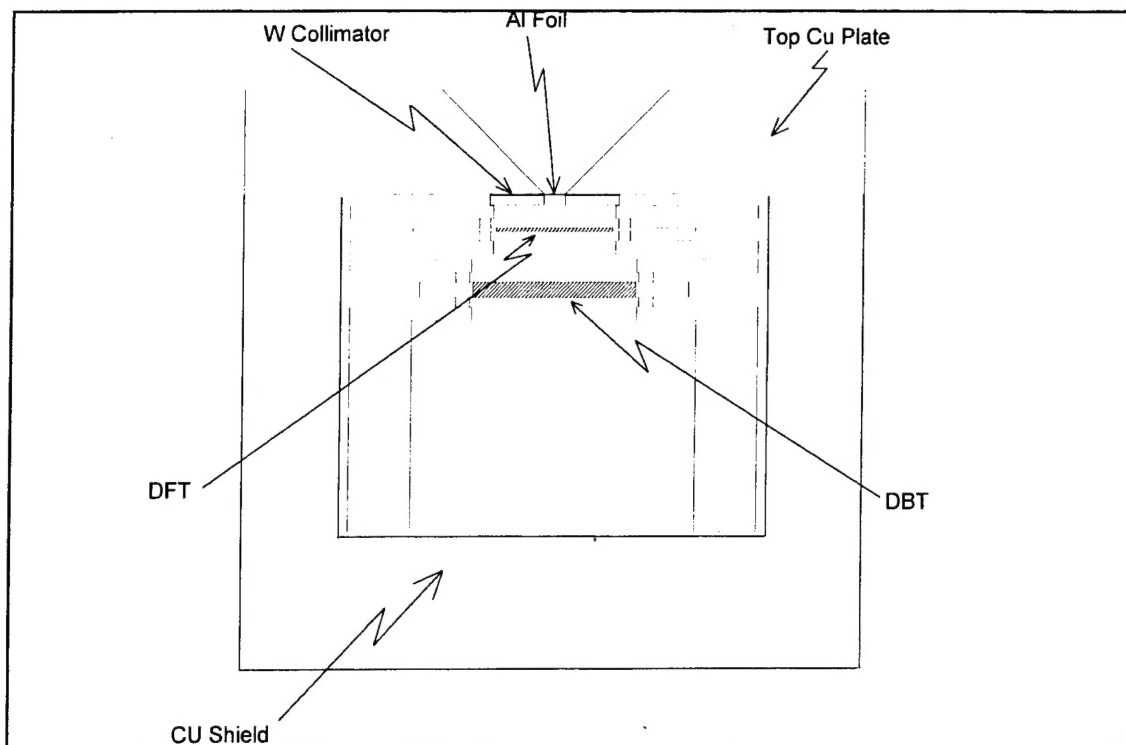
Figure 1. Schematic Cross-Section of the CEASE Telescope

In the passage through the telescope, the incident particles first encounter the 0.0009 cm thick Al degrader foil which stops protons with energies below about 2 MeV and electrons below about 50 keV. The transmitted electrons are strongly scattered in angle after traversing the foil. A secondary purpose of the foil is to make the telescope **light-tight**, since the telescope detectors are sensitive to visible light. The telescope entrance aperture is defined by the opening in the 0.5 mm thick tungsten (W) collimator. The present CEASE instrument has an 0.023 cm radius aperture. Other aperture sizes can be used, depending on the expected particle fluxes. Particles then strike the DFT and, if energetic enough, the DBT. The pulse heights from the detectors are analyzed and the energy of the incident particle is determined from this analysis.

4

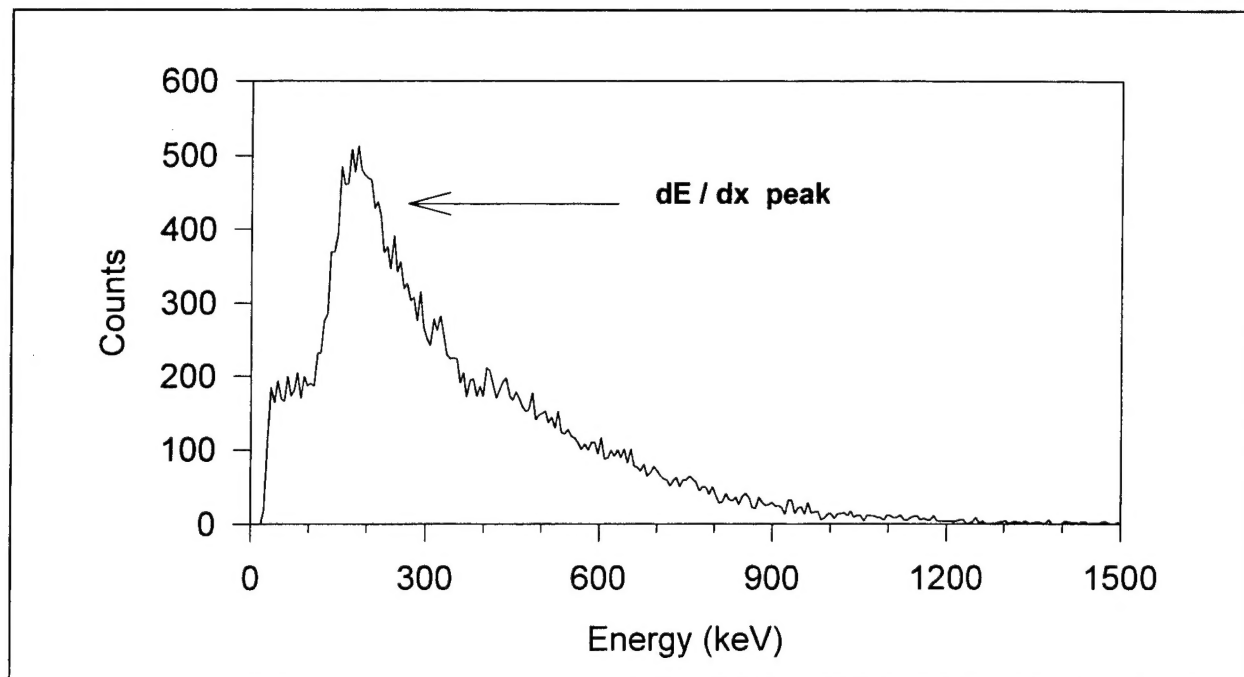**Figure 2. Electron Spectrum from Sr/Y Source (S-3950 detector).**

3. PRELIMINARY PROTON CALIBRATION

A preliminary proton test of the CEASE dosimeter was carried out at Harvard Cyclotron Laboratory. The response of the telescope to incident, monoenergetic proton beams was measured a variety of energies ($29 \leq E \leq 149$ MeV) and angles ($0° \leq \theta \leq 90°$). The experimental results, together with theoretical calculations, were used to validate the design of the dosimeter sensors.

3.1 Depletion Depth Measurement

In order to use a detector as a dosimeter, it is necessary to know its sensitive volume (area x depletion depth). Photodiode manufacturers provide nominal values of the depletion depth, but, since the proper operation of the photodiode as a light detector does not depend on this parameter, these values are often in error and vary with applied bias voltage. It is, therefore, necessary to measure the depletion depth of the photodiodes to be used in CEASE dosimeters. A simple method of making this measurement using a radioactive source ^{90}Sr has been developed and used on the CEASE detectors.

The electron energy spectrum of ^{90}Sr is continuous and extends out to the source endpoint of 2.25 MeV. Most of the emitted electrons have energies in excess of 900 keV. The shape of the energy spectrum measured with a solid state detector (see Figure 2, Hamamatsu S-3950 photodiode) is characterized by a smooth curve tending to 0 for energies above 1 MeV. Superimposed on the smooth shape is a well pronounced low energy "dE/dx" peak. The smooth curve is due to electrons that undergo significant scattering and deposit large amounts of energy in the detector. The peak is due to fast electrons that travel in nearly straight lines through the
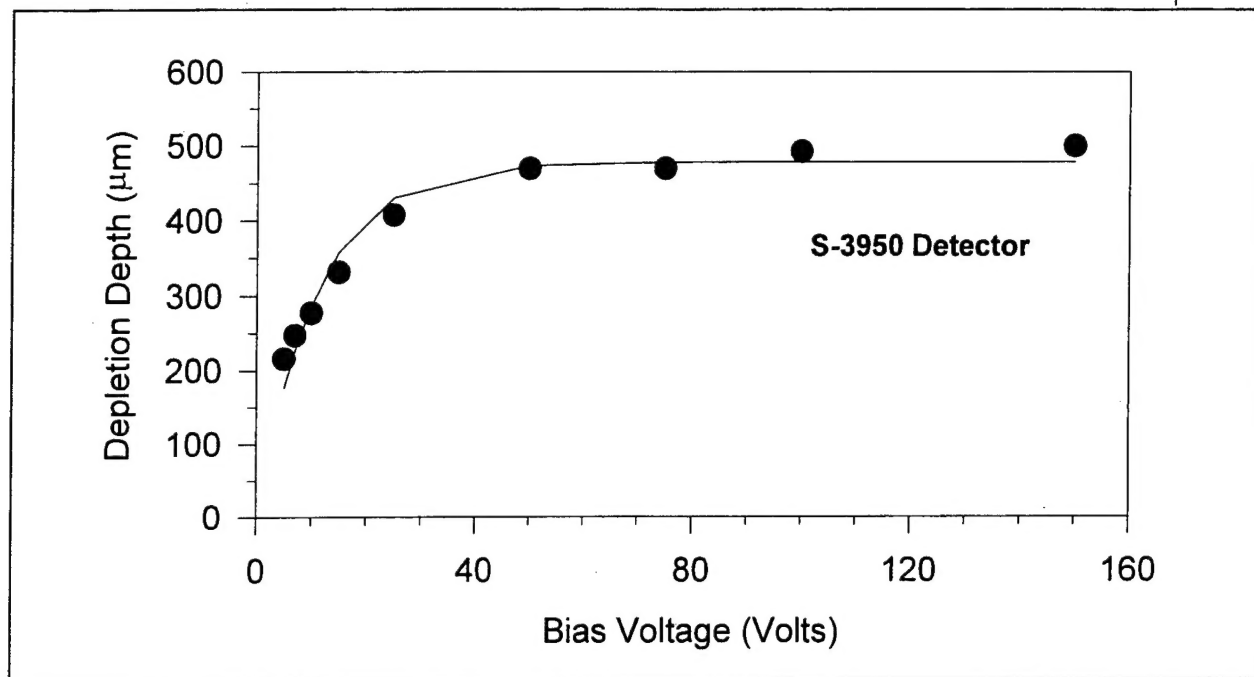
5

Figure 3. Depletion Depth vs. Bias Voltage.

detector. Since fast electrons (energies above 500 keV) have a nearly constant rate of energy loss per unit length in a material (dE/dx = 3.7 MeV/cm), all fast electrons, regardless of energy, contribute to the same narrow peak.   The detector depletion depth, t, can be calculated from the peak centroid energy, E_c: $t = E_c / 3.7$, with E_c in MeV and t in cm. This procedure can also be performed with monoenergetic electron beams, where the dE/dx value can be determined from data tables with more accuracy.

Hamamatsu S-3950 photodiodes have been chosen for use as the dosimeter detectors on CEASE. These detectors have the largest depletion depth (about 500 μm) of any commercially available photodiodes. This large depletion depth increases the typical fast-electron energy loss in the detectors to about 180 keV, well above electronic noise threshold and, thus, aids in the detection and identification of incident electrons.

Photodiode depletion depth varies with applied bias voltage. This variation is shown in Figure 3 for the S-3950 photodiode. The nominal operating voltage is 125 V so that even large increases in leakage current, which would reduce the effective bias voltage, should have no significant effect on the detector depletion depth. Photodiode leakage current will increase on-orbit with radiation damage. The S-3950 photodiodes were not available at the time the initial dosimeter proton beam tests were carried out. Two other photodiodes were used: EG&G YAG-200 with a measured depletion depth of about 330 μm and Hamamatsu S-3071 with a measured depth of 170 μm.
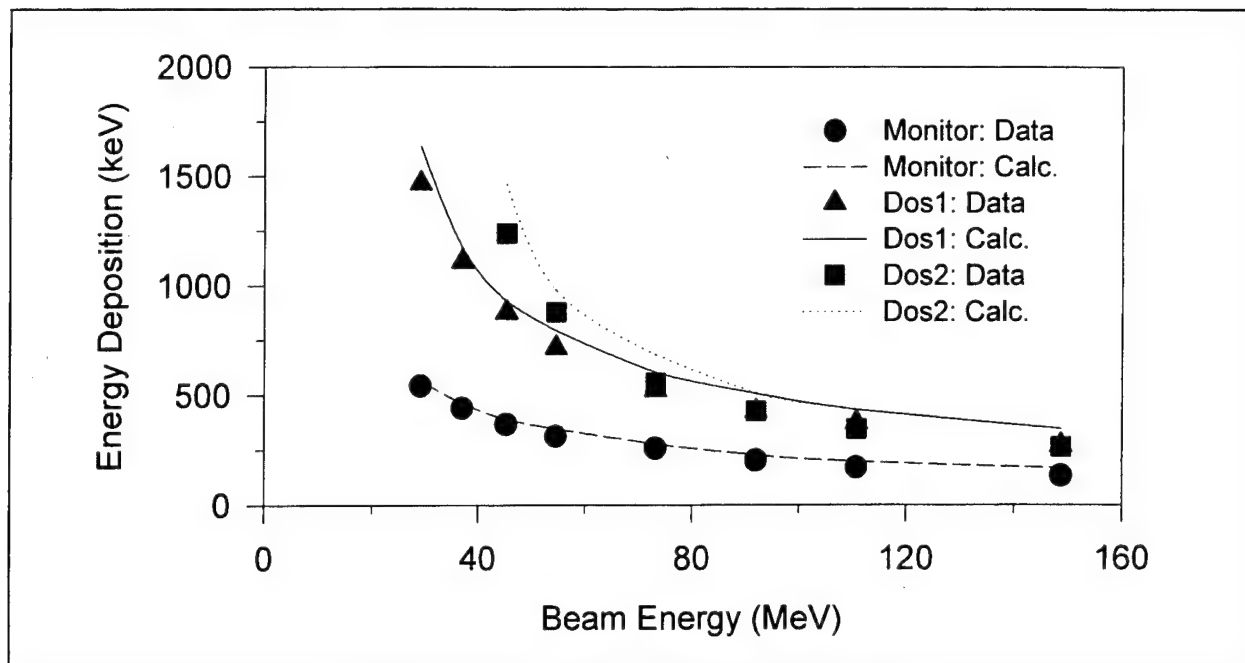
6

Figure 4. Energy Deposition by Protons.

3.2 Experimental Setup

The proton response work was carried out at the 160 MeV proton accelerator at the Harvard Cyclotron Laboratory. The machine produces a monoenergetic beam at 160 MeV. The beam energy is degraded to a variety of energies between 29 and 150 MeV using a calibrated, standard set of plastic and lead degraders. The CEASE prototype instrument was mounted on a rotary table 65 in downstream of the beam collimator exit aperture in the center of the beam A monitor detector (158 μm thick solid-state detector) could be moved directly in front of the CEASE instrument or moved to its normal location, 1.7 in away from the beam axis. In the first position, the monitor was used to measure the beam intensity at the CEASE location. In the normal position, the monitor viewed the scattered beam several degrees off axis.

The CEASE prototype consisted of three photodiode detectors: two EG&G YAG-200 units (Dos1 behind 0.08 in of Al shielding and Dos2 behind 0.25 in of Al shielding) and a Hamamatsu S-3071 unit behind 0.08 in of Al shielding. Due to time constraints, very little data was collected with the S-3071 unit and this detector will not be included in the subsequent analysis. All detectors were energy calibrated using a variety of x-ray and γ-ray sources.

3.3 Experimental Results and Calculations

The measured and calculated energy losses in the monitor detector and the two dosimeter detectors are shown plotted in Figure 4. The data points are the centroids of the sharp proton energy-loss distributions in the detectors with the beam normal to the CEASE instrument. The calculated values were obtained using a custom-written computer program which calculated the

7

energy losses in the detectors using the known CEASE prototype geometry and the data in the range-energy tables of Janni (Ref. 1). The calculations are in good agreement with the data.

The energy loss in the detector as a function of angle of incidence of the high-energy proton should vary as the path length of the particle in the detector, as $1/\cos(\theta)$. The measured, cosine-corrected peak energies at a beam energy of 110 MeV for Dos1 are within 5% of the 0° peak for angles up to 60°. At 75°, the cosine-corrected energy deposition is about 10% above the 0° value. At larger angles, it is difficult to measure the peak of the energy deposition because the protons are striking the detector nearly "edge on" and the event count rates are very low.

The measurement of angular response of the dosimeters was not successful due to the difficulty in obtaining a proper beam-flux normalization. The single, off-axis monitor detector was not capable of fully characterizing the beam, which appeared to wander in angle and whose flux varied strongly with time. An improved beam-flux monitoring system will be developed for the final CEASE proton calibration.

4. PRELIMINARY ELECTRON CALIBRATION

A preliminary electron calibration of the CEASE telescope was carried out at the Phillips Laboratory Dynamitron accelerator facility. The response of the telescope to incident, monoenergetic electrons beams was measured a variety of energies ($65 \leq E \leq 700$ keV) and angles ($0° \leq \theta \leq 100°$). The experimental results, together with theoretical calculations, were used to validate the design of the telescope.

4.1 Experimental Setup

The CEASE telescope assembly (see Figure 1) and two beam monitor detectors were mounted inside the 15 in diameter vacuum chamber attached to the exit port of the Dynamitron accelerator. The electron beam entered the chamber, traversed a 1 mil thick Titanium (Ti) scattering foil and irradiated the telescope and the monitor detectors. During the tests, the telescope was not integrated into the CEASE instrument but was tested independently of the CEASE electronics and mechanical enclosure. The telescope detector signals were processed with external, commercial NIM electronics.

The telescope was attached to a rotary table, with the center of rotation directly underneath the front detector (DFT). The telescope aperture was 50 cm from the scattering foil (see Figure 5). One beam monitor (MonA) was mounted near the edge of the rotary table at a right angle with respect to the telescope. With the table at 0°, the telescope aperture was normal to the beam axis. As the table was rotated, the telescope aperture rotated in the beam. As the table was rotated to -90°, MonA crossed in front of the telescope and its aperture became normal to the beam axis. In this position, MonA was 5 cm closer to the scattering foil than the telescope. A second monitor detector (MonB) was located 5 cm directly above the telescope on a stationary mount that was not affected by the rotation of the table.

The monitor detectors were 20 mm^2, 170 μm thick p-i-n photodiodes. Each had a 0.15 cm thick Cu collimator with an 0.20 cm diameter hole (0.0316 cm^2 area). The collimator thickness was equal to the range of 2 MeV electrons. MonB was used to provide angle-to-angle normalization for the telescope data, while MonA was rotated into the beam to provide absolute beam intensity normalization. Before the start of the beam experimental work, all detectors were energy calibrated using a ^{133}Ba source.

4.2 Beam Intensity Determination

At each energy, the relative angle-to-angle beam normalization was obtained from the MonB counting rate. MonB was mounted in a fixed position 50 cm from the scattering foil and 5 cm above the beam axis (6° with respect to the axis). This allowed the MonB count rate to normalize the telescope response data, as the telescope was rotated in angle. However, since
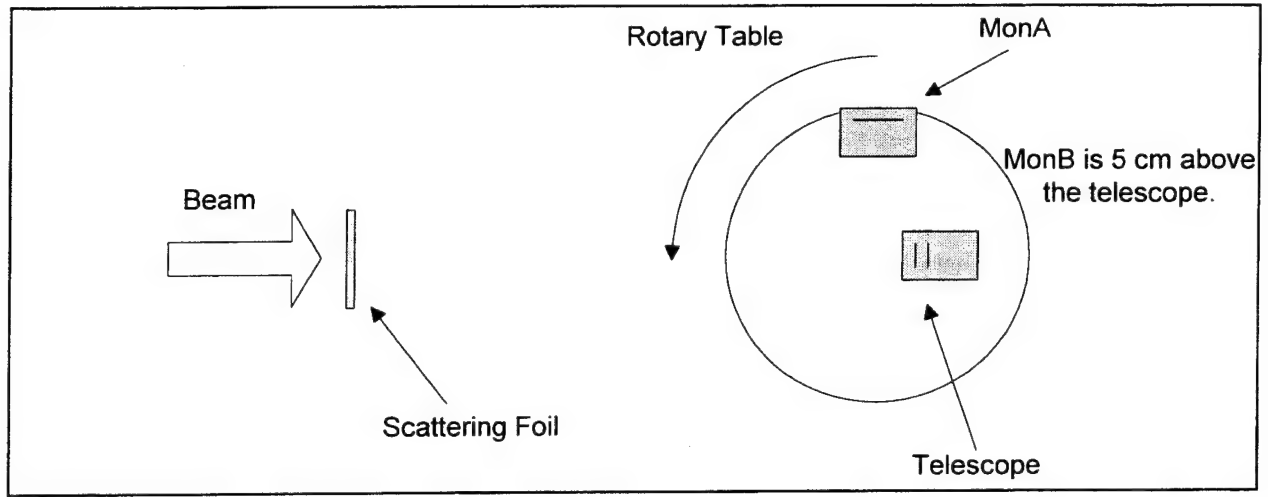
Figure 5. Schematic Diagram of the Experimental Setup.

MonB was not located along the beam axis, and the angular intensity profile of the beam was not known, it could not be used for absolute beam flux measurements.

The absolute beam flux measurement was determined using the MonA detector. At each energy, MonA was rotated into the beam axis and the count rate of both MonA and MonB were recorded. The electron flux along the beam axis, B, is then given by:

$$B = \frac{MonA}{A_{MonA} \cdot t} \quad (\text{electrons} \cdot \text{cm}^{-2} \cdot \text{sec}^{-1}), \tag{1}$$

where A_{MonA} is the MonA aperture area in cm^2 and t is the duration of the measurement in seconds. A ratio of the monitor count rates (R_m) is derived from the data with

$$R_m = \frac{MonA\,(\theta = -90°)}{MonB\,(\theta = -90°)} \quad . \tag{2}$$

Since the ratio R_m accounts for angular scattering of the beam in the Ti scattering foil, it only depends on beam energy. Thus, MonB counts at an arbitrary angle θ can be converted to an absolute beam flux measurement by combining eqs. (1) and (2):

$$B = \frac{MonB \cdot R_m}{A_{MonA} \cdot t} \quad (\text{electrons} \cdot \text{cm}^{-2} \cdot \text{sec}^{-1}). \tag{3}$$

A listing of R_m values measured during the experiment is shown in Table 1. The increase of the R_m values with increasing energy reflects the fact that the electron angular scattering in the foil decreased with increasing energy.

10

Equation (3) is valid for the telescope if the beam flux at the MonA aperture location is the same as the flux at the telescope aperture location. Since MonA aperture is 5 cm closer to the scattering foil than the telescope aperture, and the beam is diverging in angle from the point of impact on the foil, it is possible that the flux/unit area is different at the two locations. The maximum difference would occur if the electrons were scattered isotropically from the foil and the flux/unit area varied inversely with the square of the distance from the foil. In this case the flux density at the telescope would be $(45 \text{ cm} / 50 \text{ cm})^2 = 0.81$ of the flux density at MonA. In fact, the flux density at the telescope must be much closer to the MonA flux density because of the detector-beam dynamic effects. Both apertures subtend a very small opening half-angle (0.026° for the telescope and 0.12° for MonA), while the beam spot is about 2 x 2 mm^2 in size and it moves randomly over a foil area of a few square millimeters with a 60 Hz frequency. The result of the small apertures and the dynamic beam spot effects is to average the flux incident on the two detectors over an angle large compared to their aperture sizes. This would tend to make the flux density at the two locations more nearly equal.

4.3 Relative Angular Response

The relative angular response of the telescope front detector, $R_{DFT}(\theta)$, is experimentally determined using:

$$R_{DFT}(\theta) = \frac{DFT(\theta)}{B(\theta)} \cdot \frac{B(0°)}{DFT(0°)} , \qquad (4)$$

where DFT is the front detector count rate and B is the beam intensity, as given by Eq. (3). Note that R values at all energies are normalized to unity at 0°. The measured values of $R(\theta)$ for 100

Table 1. Listing of Rm and Beam Flux Values.

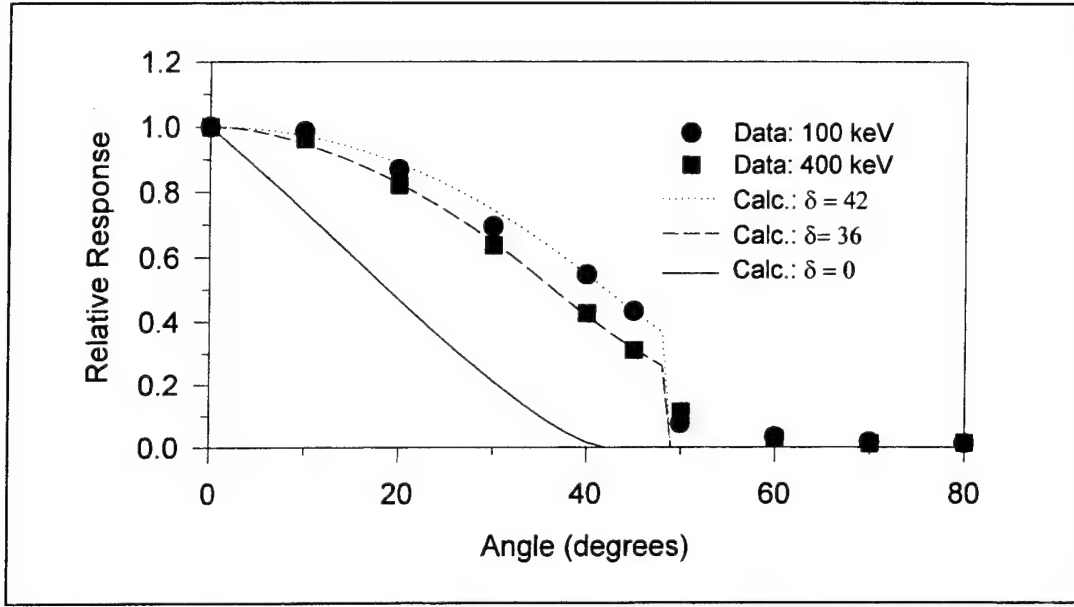| Beam Energy (keV)	R_m	Beam Flux (electrons / cm^2 / sec)
65	1.16	2.5 x 10^5
100	1.16	2.7 x 10^4
200	1.16	3.5 x 10^4
300	1.17	2.5 x 10^4
400	1.17	4.3 x 10^4
500	1.19	6.4 x 10^4
600	1.21	6.3 x 10^4
700	1.25	7.5 x 10^4

Figure 6. DFT Relative Angular Response.

and 400 keV electron beams are plotted in Figure 6. The DFT angular response does not vary appreciably from 200 to 700 keV and the 400 keV data points are typical of the DFT response above 200 keV. The lines plotted in Figure 6 are results of a simple calculation, described below, designed to qualitatively reproduce the DFT angular response.

The angular DFT response is determined by an interplay of three mechanical elements: a) the cone-shaped opening in the copper telescope cover plate, b) the aperture in the tungsten (W) collimator, and c) the Al foil in the telescope aperture. The effects of the these elements are as follows:

1) The opening in the copper top plate limits the maximum angle of incidence of particles onto the collimator aperture to 48.9°.

2) The tungsten collimator has a thickness t = 0.05 cm, and aperture with a radius r = 0.023 cm. Thus, the collimator has the same effect as two separated coaxial circular apertures. The effective area in such a geometry, as a function of angle of incidence, $A(\theta)$, is given by:

$$A(\theta) = \begin{cases} r^2 \cos(\theta) & \text{if } 0 \le \tan(\theta) \le (R-r)/D \\ \cos(\theta)[f(r,R) + f(R,r) - g(R,r,\theta)] & \text{if } (R-r)/D < \tan(\theta) \le (R+r)/D \\ 0 & \text{if } \tan(\theta) > (R+r)/D \end{cases} \quad (5)$$

where

$$f(x,y) = x^2 \cos^{-1}\left(\frac{x^2 - y^2 + D^2 \tan(\theta)}{2 x D \tan(\theta)} \right) \quad (6)$$

12

and

$$g(x,y,\theta) = D \tan(\theta)\sqrt{\left(\frac{x^2+y^2}{2}\right)+\left(\frac{(x^2-y^2)^2}{4\,D^2\tan^2(\theta)}\right)+\left(\frac{D^2\tan^2(\theta)}{4}\right)}\ . \tag{7}$$

R and r are the larger and smaller of the two aperture radii and D is the distance between the apertures. For the case of the telescope $r = R = 0.023$ cm and $D = 0.05$ cm.

3) The Al foil (0.0009 cm thick, areal density 2.4 mg/cm^2) scatters incident electrons before they enter the collimator aperture. As a result, electrons incident at one angle are "smeared" in angle, or scattered into trajectories at a variety of angles, centered on the initial one. The typical scattering angle can be in the range of 20-40° (Ref. 2).

The predicted DFT angular response, $P_{DFT}(\theta)$, can be calculated using a simple model which assumes that electrons incident at an angle of θ, are uniformly scattered into a range of angles between $\theta - \delta$ and $\theta + \delta$. The parameter δ is adjustable and is varied to fit the data. In this model, $P_{DFT}(\theta)$ can be written as:

$$P_{DFT}(\theta) = \frac{1}{2\delta}\cdot\int_{\theta-\delta}^{\theta+\delta} A(\phi)\,d\phi\ , \tag{8}$$

where A is given by eq. (5). The lines plotted in Figure 6 show the $P_{DFT}(\theta)$ values calculated with eq. (8) for δ values of 0°, 36° and 42°. Note that if $\delta = 0$, then $P_{DFT}(\theta) = A(\theta)$. The values of δ obtained from the data are consistent with those of (Ref. 2) and, as expected, the larger δ value corresponds to the lower energy data.

The relative angular response of the DFT-DBT coincidence is shown in Figure 7. The data points are obtained from:

$$R_C(\theta) = \frac{CC(\theta)}{B(\theta)}\cdot\frac{B(0°)}{CC(0°)}\ , \tag{9}$$

where CC are the DFT-DBT coincidence counts and B is the beam intensity as given by Eq. (1). The lines plotted in Figure 7 are results of calculations using Eq. (8) with $\delta = 0°$ and 36°. As can be expected, the response is broader in angle than the $\delta = 0°$ calculation result and very similar in shape to the DFT response. Electrons suffer large angular scattering in the DFT detector, so that the angle of incidence onto the DFT has very little effect on the angular response of the DBT detector. Thus, the angular DBT response should closely follow the DFT angular response.
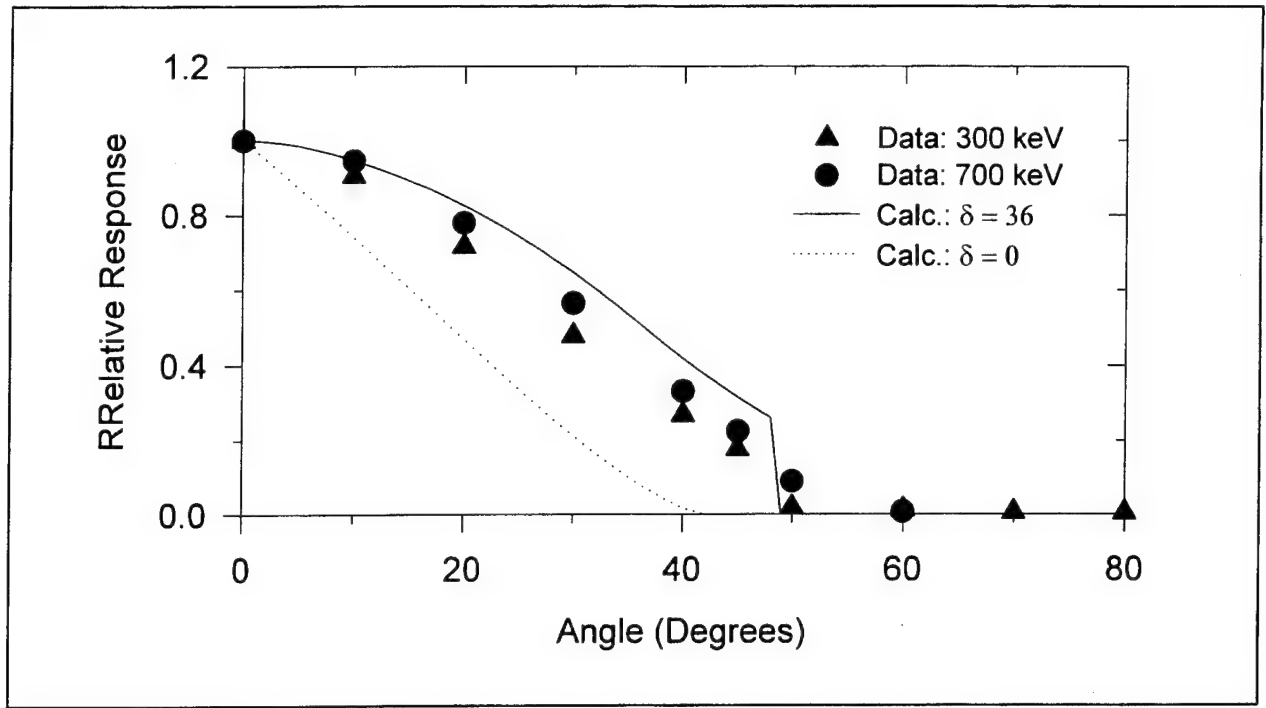
13

Figure 7. DFT-DBT Coinc. Relative Angular Response.

4.4 Effective Areas and Geometric Factors

The effective area of the DFT, for a normally incident beam, varies as a function of incident electron energy. The variation occurs primarily due to electron scattering in the Al foil, which removes electrons from the collimator acceptance cone. The purely geometrical DFT sensitive area, A_{G-DFT}, is determined by the collimator aperture (radius = 0.023 cm) because the DFT active area is large enough (radius = 0 .282 cm) so that any particles that traverse the collimator will strike the DFT. The collimator area is 1.64×10^{-3} cm^2 and this is also the value of A_{G-DFT}.

The experimentally determined, energy-dependent, effective DFT area, $A_{DFT}(E)$, is determined using

$$A_{DFT}(E) = \frac{DFT \cdot A_{MonA}}{MonB \cdot R_M} , \qquad (10)$$

where $A_{MonA} = 0.0316$ cm^2 (MonA collimator area) and DFT and MonB are the respective counts in the two detectors (DFT counts include only events with the deposited energy above 30 keV in DFT). Similarly, we define the effective DBT, $A_{DBT}(E)$, and DFT-DBT Coincidence, $A_C(E)$, areas using

$$A_{DBT}(E) = \frac{DBT \cdot A_{MonA}}{MonB \cdot R_M} , \qquad (11)$$

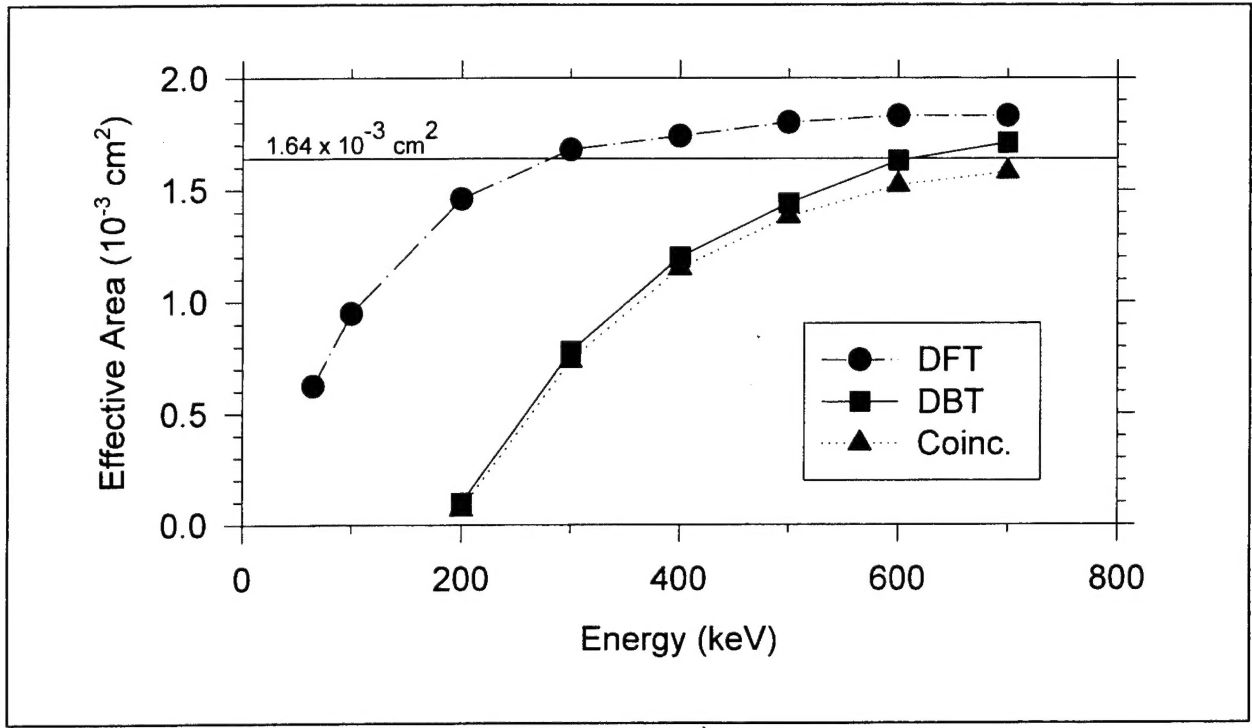with DBT counts requiring a minimum of 30 keV of energy deposition, and

Figure 8. Energy Dependent Effective Areas.

$$A_C(E) = \frac{C \cdot A_{MonA}}{MonB \cdot R_M} \, . \tag{12}$$

Experimentally determined values of the these areas are shown plotted in Figure 8. The fact that the effective areas at higher energies slightly exceed the geometrical one must be attributed to the uncertainties in the beam flux determination, primarily due to the assumption that the beam flux at the MonA location is the same as at the telescope location. The maximum error in seen in the plots in Figure 8 is less than 12%, well within the known experimental uncertainties. The increased divergence between the DBT and Coincidence effective areas at higher energies reflects the fact that high-energy electrons have a higher probability of reaching the DBT without passing through the DFT, for example, by scattering through the detector housing.

The effective 0° areas and the relative angular responses can be used to determine the energy dependent telescope effective geometrical factors. The energy dependent effective geometric factor, GF(E), is defined by:

$$GF(E) = 2\pi \int_0^\pi A(\theta,E) \sin(\theta)\, d\theta = 2\pi \int_0^\pi A_o(E)\, R(\theta,E) \sin(\theta)\, d\theta \, , \tag{13}$$

where $A(\theta,E)$ is the effective area as a function of angle, A_o is the measured 0° area and $R(\theta,E)$ is the measured relative angular response. The experimentally determined GF(E) values are shown plotted in Figure 9 (lines are drawn to guide the eye). For comparison, the geometric factor calculated using A_{G-DFT} and the $\delta = 0$ relative angular response from Eq. (5), GF_g, is 0.76×10^{-4} cm^2-sr. GF_g is smaller than the high-energy limit of GF(E) because electron scattering in the Al
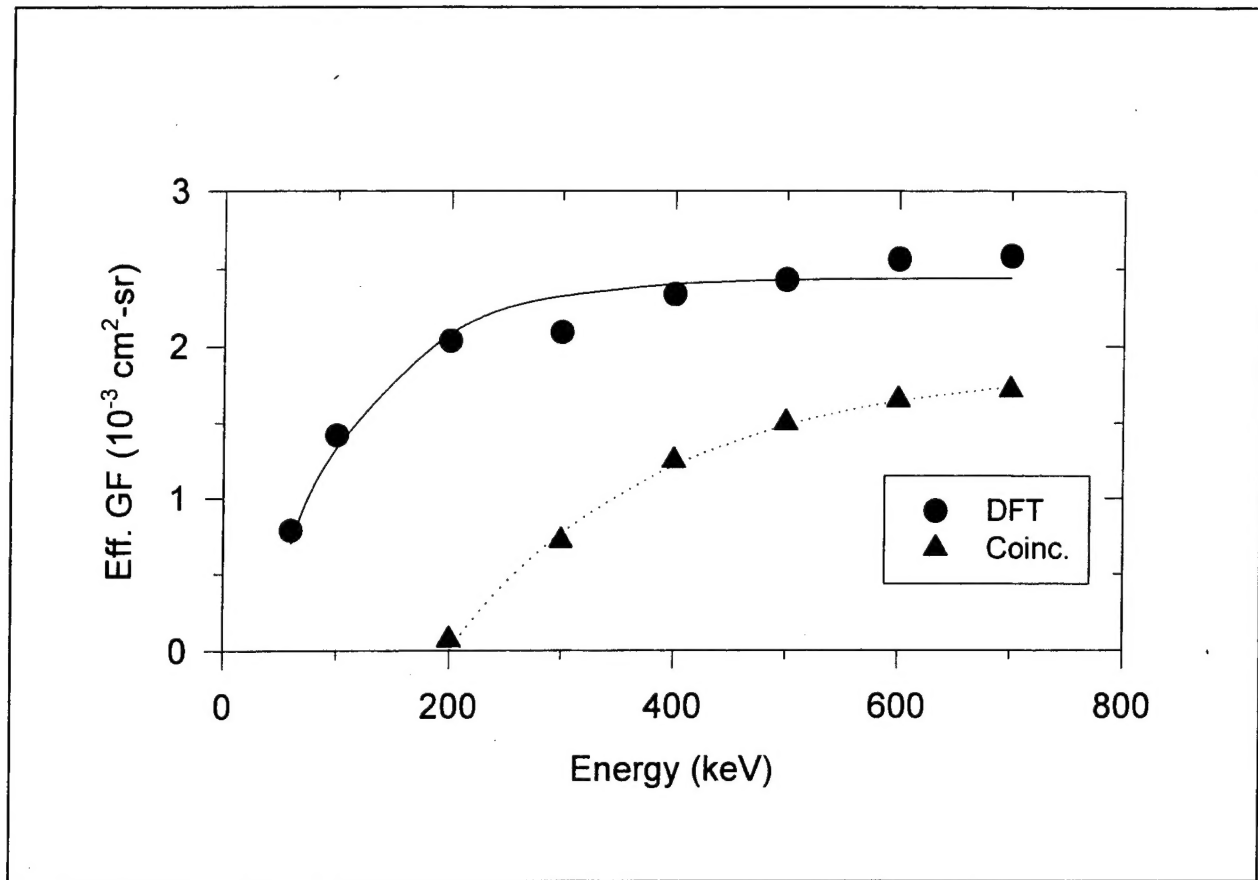
15

Figure 9. Effective Geometric Factors.

foil broadens the telescope angular response relative to what it would have been without the foil (see Figure 6). If the foil had been placed on the downstream end of the collimator, the telescope angular response would have been very similar to the $\delta = 0$ curve calculate using Eq. (5) and the high-energy GF(E) limit would be GF_g. Placing the foil on the upstream side of the collimator results in a higher effective geometric factor (a disadvantage if incident electron flux is high), but it makes the telescope angular response largely independent of the collimator geometry (an advantage if several instruments with different collimators are to be flown).

5. CONCLUSIONS AND FUTURE PLANS

The results of the preliminary CEASE calibration work indicate that the performance of the dosimeters and the telescope in response to monoenergetic particle beams can be well reproduced by calculations based on the detector geometry and known electron and proton scattering properties. This agreement gives us confidence that our theoretical models of the CEASE instrument are correct and that we can use them to predict the instrument's response in the complex space environment. The experimental work carried out so far is preliminary, it was done with prototype sensors and external electronics, and must be extended in order to fully characterize the response of the CEASE instrument.

The following experimental work is planned for the final year of the project:

1) High Energy Protons - We will return to HCL (29 to 150 MeV protons) with a flight model CEASE a) to complete the energy deposition studies already started, b) to study the angular response of the dosimeters to high-energy protons, including rear and side entry particles, and 3) to characterize the telescope response to high-energy protons. An improved beam flux monitoring system will be developed for this experiment.

2) Low Energy Electrons - We will return to the PL Dynamitron (0.1 to 1.1 MeV) accelerator to complete the telescope calibration work with the CEASE internal electronics. Geometric factors for all electron channels will be measured. We will also measure dosimeter detector depletion depths using monoenergetic electron beams.

3) High Energy Electrons - We will use the electron linac at the Rensselaer Polytechnic Institute (5 to 20 MeV electrons) to calibrate the dosimeter and telescope response to high energy electrons. CEASE response will be studied at a variety of angles including rear and side entry particles.

4) Low Energy Protons - We will use the Van de Graaff accelerator at the University of Massachusetts at Lowell (1 to 5 MeV protons) to study the telescope response to low-energy proton beams.

In addition, we will conduct a detailed comparison of the measured telescope response to electrons with a set of Monte Carlo calculations performed by the SAIC group. These calculations are an important element of the CEASE on-orbit response characterization and, therefore, should be thoroughly validated. Data to be collected at the Dynamitron will allow this validation to be performed.

6. REFERENCES

1 -   Janni, J. F., "Calculations of Energy Loss, Range, Pathlength, Straggling, Multiple Scattering, and the Probability of Inelastic Nuclear Collisions for 0.1 to 1000 MeV Protons," AWFL-TR-65-150.

2 -   Seltzer, S. M. and M. J. Berger, "Transmission and Reflection of Electrons by Foils," NIM, **119,** (1974), p. 157-176.